Investigation of a cavitation bubble between a rigid boundary and a free surface

Peter Gregorčič,[a] Rok Petkovšek, and Janez Možina
Faculty of Mechanical Engineering, University of Ljubljana, Aškerčeva 6, 1000 Ljubljana, Slovenia

(Received 25 August 2007; accepted 13 September 2007; published online 7 November 2007)

When a high-intensity laser pulse is focused into a liquid the energy is converted into mechanical energy via an optodynamic process. The conversion starts with plasma formation; this is followed by shock-wave propagation and the expansion of a cavitation bubble. A cavitation bubble developed near boundaries results in an asymmetrical collapse, with the generation of a liquid jet during the bubble's rebound. In the case of a free surface this liquid jet is directed away from the surface and the oscillation times are prolonged. On the other hand, in the case of a rigid boundary, the liquid jet is directed toward the boundary and the oscillation times are shortened. We present measurements of a cavitation bubble oscillating between a free surface and a rigid boundary using deflections of a laser beam as the optical probe. Shadow photography was used simultaneously as a comparison during the experiments. With the beam-deflection probe we also measured the shortening of the oscillation times near a free surface as well as the prolongation of oscillation times near a rigid boundary. In order to explain this shortening of the cavitation-bubble oscillation times near a free surface, Rayleigh's model was extended and compared with our experimental results. © *2007 American Institute of Physics*. [DOI: 10.1063/1.2805645]

I. INTRODUCTION

Laser-induced cavitation is an optodynamic process where the optical energy of a high-intensity laser pulse is converted into the mechanical energy of dynamic phenomena, i.e., the expansion of a plasma, the propagation of a shock wave and the growth of a cavitation bubble. For such a process a laser pulse in the nanoseccond range, focused into distilled water, is usually used[1–23] to achieve highly localized ionization of the liquid media, leading to plasma formation. Rapid energy deposition during the optical breakdown causes rapid temperature and pressure increases within the plasma, thereby initiating its explosive expansion.[19] As a result the optical breakdown is followed by the expansion of the shock wave and the growth of the cavitation bubble. When a cavitation bubble expands to its maximum volume it is nearly empty.[24] As a consequence it starts to collapse due to the pressure of the surrounding liquid. However, after this collapse the bubble rebounds and the process repeats itself in the form of bubble oscillations. It is known that such a collapse in an infinite liquid is spherical and can be roughly described by the Rayleigh–Plesset model.[25,26] On the other hand, a cavitation bubble developed near a boundary results in an asymmetrical collapse.[27] Under suitable conditions the deformation during the latter type of collapse near an interface results in the generation of a liquid jet[28] and the direction of this liquid jet during the collapse phase is determined by the physical properties of the boundary.[29] If the interface is a rigid boundary, the jet is directed toward the wall, an oscillating bubble migrates toward the surface and the oscillation times are prolonged.[4,9,10,16,28,30] However, in the case of a bubble collapse near a free surface, the jet is directed away from the free surface, the bubble migrates away from the boundary during the collapse phase, and the oscillation times are shortened.[11,16,29,30]

The interest in cavitation-bubble dynamics near boundaries mainly arose from bubbles' destructive action on surfaces. Historically, the search for the origin of the erosion by cavitation bubbles was the motivation for investigating bubble dynamics.[9] Cavitation erosion was investigated with laser-induced[2,9,10,14,17] and spark-generated[28] bubbles as well as acoustically generated[31] cavitation. Furthermore, the investigation of laser-induced bubble dynamics is motivated by the important role of cavitation bubbles in various medical applications for laser surgery, such as intraocular photodisruption,[5] laser lithotripsy,[32] and the micromanipulation of individual cells.[33,34] Recently, there have also been some studies related to biomedicine, where the cavitation of the microbubbles can be used to enhance membrane permeabilization and molecular uptake (sonoporation).[35,36]

Optical methods are normally used to investigate cavitation-bubble dynamics and the shock waves that follow as the bubble collapses because of their ability to measure bubble and shock-wave dynamics in the vicinity of the breakdown region.[22] Basically, there are three different types of optical methods for measuring bubble dynamics. Two of them are based on a scanning procedure and therefore require a measuring process with good repeatability. The first type is represented by methods such as shadow photography[6,7] or schlieren photography,[28,37] where the whole two-dimensional (2D) image of the bubble can be observed at once. However, the measuring process should be carried out at different times relative to the occurrence of the breakdown in the case of a dynamic investigation of the bubble. Another type of scanning method is based on a laser beam-deflection probe (BDP).[3,18,21–23] Here, measurements

[a]Electronic mail: peter.gregorcic@fs.uni-lj.si

 © 2007 American Institute of Physics

Downloaded 08 Nov 2007 to 193.2.7.100. Redistribution subject to AIP license or copyright, see http://jap.aip.org/jap/copyright.jsp

are made at different positions of the laser probe relative to the breakdown region, representing the origin of the cavitation bubble. In this case the whole time evolution of the bubble can be measured using a single shot, but only at a single point in space. Therefore, from one BDP signal information on bubble expansions, collapses, and also the corresponding shock waves can be obtained. The third type is represented by high-speed photography with up to 5×10^6 frames per second.[1,2,4,9,10,12,13,16,19,31,38] This method makes possible dynamic 2D measurements of the bubble in a single shot, but the experiment requires a very sophisticated environment.

In our study we used a scanning procedure based on the BDP method[23] for our investigation of the bubble dynamics between a rigid boundary and a free surface. However, for data verification reasons we simultaneously employed shadow photography. Since a single BDP signal includes information on the shock waves emitted after the breakdown and during the bubble's collapses, oscillation times can be deduced by analyzing the signal. For this reason we also investigated the oscillation times of the cavitation bubble versus the distance between the breakdown region for the rigid boundary as well as the free surface.

II. THEORY

The collapse of a spherical bubble in an infinite liquid can be roughly described by Rayleigh's model if we consider an incompressible and inviscid liquid as well as constant pressure for the liquid and the inside of the bubble during the collapse.[25] With these assumptions the Rayleigh collapse time T_C can be easily deduced from the law of energy conservation

$$T_C = 0.915 R_{\max}\sqrt{\frac{\rho}{p_0}}. \tag{1}$$

Here ρ and p_0 are the liquid's density and the liquid's pressure, respectively. However, since the rigid boundary causes a prolongation of the collapse time, Eq. (1) is no longer appropriate. According to Rattray's[39] perturbation theory of the Rayleigh's model, the prolongation factor κ_p, defined as the ratio between the collapse time of a bubble collapsing near a rigid boundary T_{CR} and the Rayleigh's collapse time T_C, can be roughly described by the equation

$$\kappa_p = \frac{T_{\mathrm{CR}}}{T_C} = 1 + \frac{0.205}{\gamma}. \tag{2}$$

Here $\gamma = s/R_{\max}$ is a dimensionless distance,[2,4,28] where s and $R_{\max}$ are the distance of the center of the bubble from the boundary and the bubble's maximum radius, respectively.

In the case of a free surface, the collapse time of the bubble is shortened. Therefore, in this case we can talk about a shortening factor κ_s, defined as the ratio between the collapse time of a bubble oscillating near a free surface T_{CF} and the Rayleigh collapse time T_C. In order to explain this shortening, we extended Rayleigh's model for the case of an oscillating bubble in the vicinity of a boundary between two liquids, as shown schematically in Fig. 1. In the present approach we neglect the surface tension, the viscosity and the mass transfer across the bubble boundary. We also assume a uniform and constant temperature and take the pressure inside the bubble to be zero. We further assumed that the pressure inside both liquids is constant and that it is equal to p_0 during the collapse. Using these assumptions the collapse time of an oscillating bubble with a radius $R_s(t)$ can be derived from Rayleigh's theory as follows. The incompressibility links $R(t)$ and $R_s(t)$, while the radial liquid velocity $\dot{r}(r > R)$ can be obtained from the continuity equation $\nabla\cdot\mathbf{v}=0$,

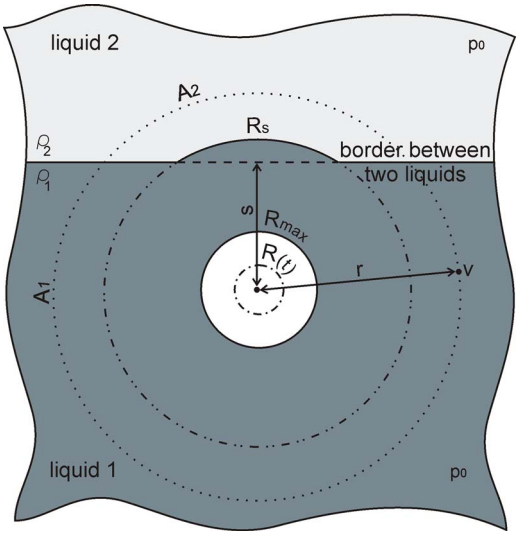

FIG. 1. (Color online) Schematic description of the extended Rayleigh model for a bubble oscillating near a boundary between two liquids with densities ρ_1 and ρ_2.

$$R_s(t) = [s^3 + R^3(t)]^{1/3}, \tag{3}$$

$$\dot{r} = \frac{\dot{R}R^2}{r^2}. \tag{4}$$

Here $R_s(t)$ is the radius of a sphere centered around the bubble and filled only with liquid 1, while s is the distance between the center of the bubble and the boundary (see also Fig. 1). The kinetic energy of the liquid is

$$E_{\mathrm{kin}} = \frac{1}{2}\int_R^\infty \dot{r}^2 dm = \frac{1}{2}\dot{R}^2R^4\int_R^\infty \frac{dm}{r^4}. \tag{5}$$

The sphere which presents the liquid at any distance r should be divided into two parts: the part that lies in the liquid 1, with the density ρ_1, and the part that lies in the liquid 2, with the liquid density ρ_2 (see also Fig. 1). The first part of the sphere has an area A_1, while the second part has the area A_2. Therefore, the kinetic energy, defined with Eq. (5), can be expressed as

Downloaded 08 Nov 2007 to 193.2.7.100. Redistribution subject to AIP license or copyright, see http://jap.aip.org/jap/copyright.jsp

$$E_{\mathrm{kin}} = \frac{1}{2}\dot{R}^2R^4\left[\rho_1\int_R^{R_s}\frac{4\pi r^2}{r^4}dr + \rho_1\int_{R_s}^{\infty}\frac{A_1}{r^4}dr + \rho_2\int_{R_s}^{\infty}\frac{A_2}{r^4}dr\right]$$

$$= \frac{1}{2}\dot{R}^2R^4\left[\rho_1\int_R^{R_s}\frac{4\pi r^2}{r^4}dr + \rho_1\int_{R_s}^{\infty}\frac{2\pi r(r+s)}{r^4}dr + \rho_2\int_{R_s}^{\infty}\frac{2\pi r(r-s)}{r^4}dr\right]$$

$$= 2\pi\rho_1\dot{R}^2R^3\left[1 + \frac{(\alpha-1)}{4}\frac{2(1+s^3/R^3)^{1/3} - s/R}{(1+s^3/R^3)^{2/3}}\right]. \quad (6)$$

Here we introduced a dimensionless parameter $\alpha=\rho_2/\rho_1$, showing the ratio between the density of both liquids.

The potential energy is given by integrating the pressure work pdV over the volume traversed by the surface of the bubble

$$E_{\mathrm{pot}} = \frac{4\pi R^3}{3}p_0. \quad (7)$$

The energy conservation $E_{\mathrm{kin}}+E_{\mathrm{pot}}=E_0$, where E_0 is identified with the potential energy at the bubble's maximum radius R_{max} gives

$$\dot{R} = \sqrt{\frac{1}{1+\frac{(\alpha-1)}{4}\frac{2(1+s^3/R^3)^{1/3}-s/R}{(1+s^3/R^3)^{2/3}}}\frac{2p_0}{3\rho_1}\left(\frac{R_{\mathrm{max}}^3}{R^3}-1\right)}. \quad (8)$$

Integrating this equation from $R=0$ to $R=R_{\mathrm{max}}$ yields an analytical expression for the collapse time

$$T_{\mathrm{CF}} = \psi(\alpha,\gamma)R_{\mathrm{max}}\sqrt{\frac{\rho_1}{p_0}},$$

$$\psi(\alpha,\gamma) = \sqrt{\frac{3}{2}}\int_0^1 \frac{\xi^{3/2}\left[1+\xi(\alpha-1)\frac{2(1+\gamma^3)^{1/3}-\gamma}{4(1+\gamma^3)^{2/3}}\right]^{1/2}}{\sqrt{1-\xi^3}}d\xi. \quad (9)$$

Here ξ and γ are defined as $\xi=R/R_{\mathrm{max}}$ and $\gamma=s/R_{\mathrm{max}}$, respectively. An approximation of Eq. (9) for $\gamma\to\infty$ gives

$$\psi(\alpha,\gamma) = 0.915 + 0.093\frac{(\alpha-1)}{\gamma} + O\left(\frac{1}{\gamma}\right)^2. \quad (10)$$

For infinite liquids ($\alpha=1$), we consistently obtain the Rayleigh collapse factor $\psi(1,\gamma)=0.915$. Furthermore, when the bubble collapses near a liquid having a higher density than the liquid of the bubble's origin ($\alpha>1$), the oscillation times are prolonged. On the other hand, when the liquid near a collapsing bubble has a lower density than the liquid where the bubble collapses ($\alpha<1$), the oscillation times are shortened. However, for the case of a bubble oscillating near a free surface, $\alpha=0$. Therefore, the shortening factor for this case can be expressed as

$$\kappa_s = \frac{T_{\mathrm{CF}}}{T_C} = 1 - \frac{0.102}{\gamma}. \quad (11)$$

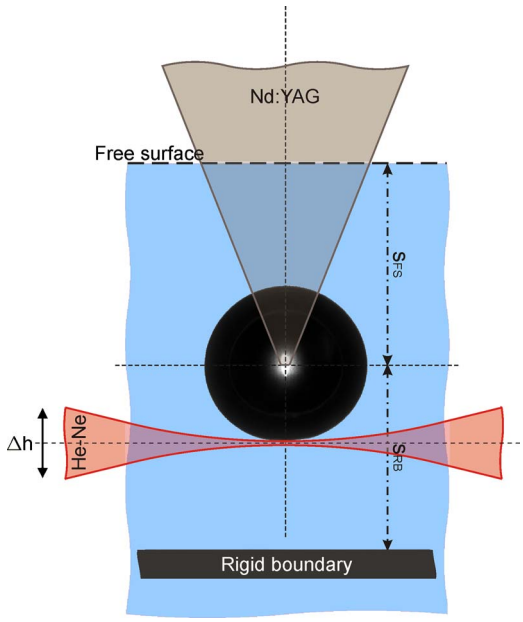

FIG. 2. (Color online) Experimental setup. The breakdown was caused by a pulsed Nd:YAG laser focused into the vessel containing distilled water and with an open top (free surface). A He-Ne laser was used as the probe beam. The optical axes of the breakdown laser lay in the probe beam's focal plane to ensure precise BDP measurements. The rigid boundary was placed under the center of the bubble. The distance between the center of the bubble and the rigid boundary (s_{RB}) and free surface (s_{FS}) was varied during the experiments.

The extended Rayleigh's model was compared with our measurements in order to explain effects observed from experimental results.

III. EXPERIMENTAL SETUP

Since a detailed description of the experimental setup and the experimental method can be found in Ref. 22, we will restrict ourselves here to a brief overview. The breakdown was induced in distilled water using a Q-switched Nd:YAG laser ($\lambda=1064$ nm) designed for ocular photodisruption. The water was held in an uncovered vessel, as shown schematically in Fig. 2. The duration of the laser pulse was 7 ns and the pulse energy used in our experiments was $8.6\times(1\pm0.03)$ mJ. The estimated waist radius of the breakdown beam in the water was ~30 μm and so the power of the pulses was in the range of 0.3–1.2 MW. The threshold energy, E_{th}, for distilled water was measured as described in Ref. 23 and was found to be $E_{\mathrm{th}}=1.1\times(1\pm0.3)$ mJ. Therefore, the dimensionless parameter β,[40] indicating the ratio between the laser energy and the threshold energy, was approximately equal to 7.8.

Two techniques were employed simultaneously during our experiments: the BDP method and shadow photography. The BDP measurements are based on the local change of the refractive index resulting from the shock wave or the cavitation bubble. When the shock-wave front or the cavitation-bubble wall crosses the path of the probe beam the refractive-index gradient causes measurable deflections of the probe.[23,41,42] These beam deflections can be detected with a quadrant photodiode—a position-sensing photodetector. The measurements presented in this paper were made by

Downloaded 08 Nov 2007 to 193.2.7.100. Redistribution subject to AIP license or copyright, see http://jap.aip.org/jap/copyright.jsp

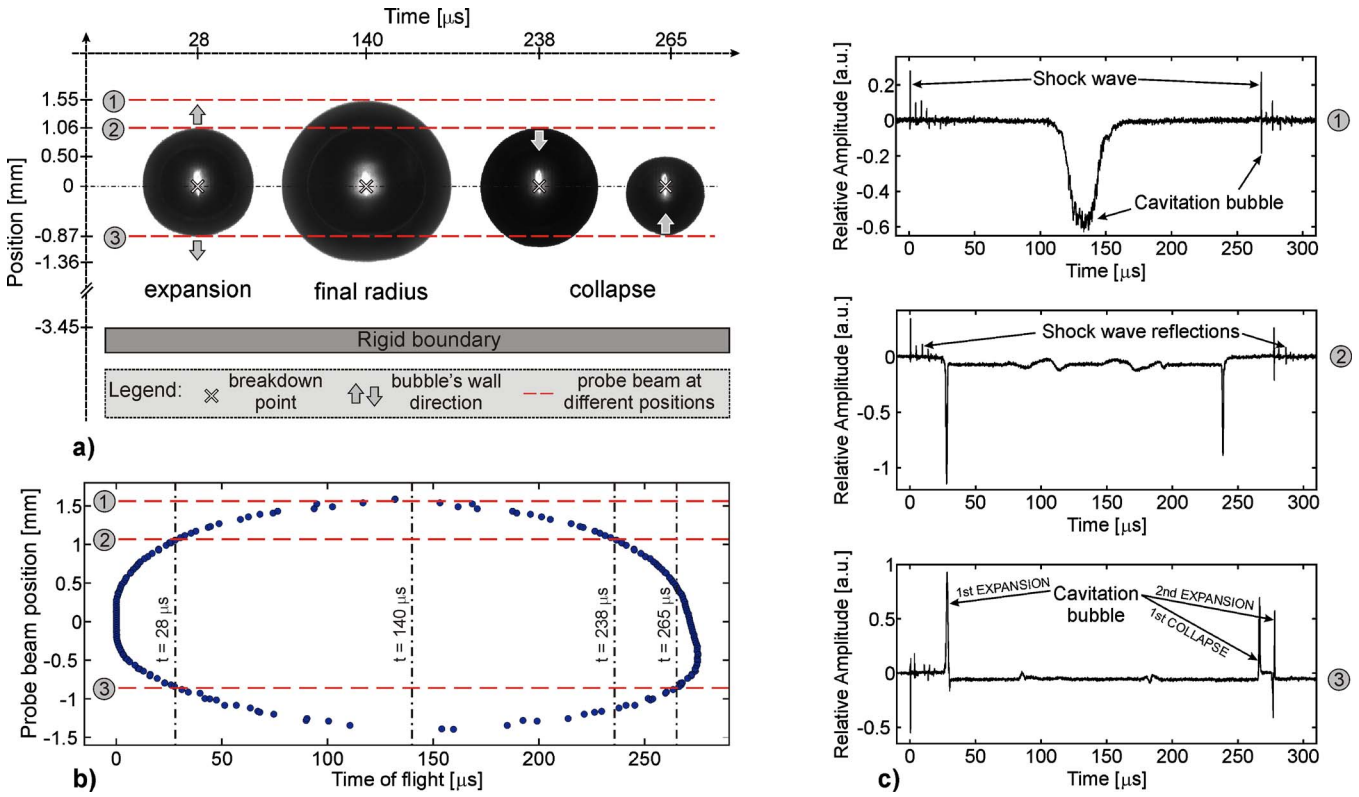

FIG. 3. (Color online) (a) Typical images taken using shadow photography during the first bubble oscillation near a rigid boundary. Three different positions of the probe beam relative to the center of the bubble are shown as dashed lines. The time is shown on the horizontal axis. (b) BDP scanning results for the first bubble oscillation. Asymmetrical collapse is clearly visible. The probe beam positions are also shown for a comparison with the shadow photography. (c) Typical BDP signals. The peak appearing shortly after the optical breakdown is a shock wave caused by the breakdown. That peak is followed by other peaks corresponding to the shock-wave reflections from the boundaries (t between ~0 and ~30 μs). Peaks caused by the bubble's expansion and the bubble's collapse are also visible. When the distance between the probe and the center of the bubble is equal to the bubble's maximum radius these two peaks merge into one (see position 1).

scanning in the vertical direction, i.e., parallel to the optical axes of the breakdown beam (see Fig. 2). The shift during the scanning was $\Delta h = 30$ μm and three measurements were made at each position of the probe beam. To ensure precise BDP measurements the optical axis of the breakdown laser should lie in the probe beam's focal plane, as shown schematically in Fig. 2. For the laser probe we employed a He-Ne laser, led through the optics to achieve a small waist radius of the beam (~3 μm). The rise time and the bandwidth of the employed quadrant photodiode were ~4 ns and ~200 MHz, respectively. By considering the speed of sound in water this roughly corresponds to the waist diameter of the probe beam. The signals from the quadrant photodiode were observed with a digital oscilloscope (500 MHz wave runner 6050A, Lecroy) controlled with specially developed software that allowed us to control the experiment automatically as well as process the data. The small beam diameter and the high-frequency bandwidth of the probe were necessary in order to achieve a high temporal as well as spatial resolution.

Shadow photography, in contrast, needs short exposure times to ensure an appropriate time resolution. For this reason a pulsed laser should be employed as the light source. In our setup we used a Nd:YAG pulsed laser with a pulse duration of 7 ns. The image was captured using a microscope equipped with a charge coupled device camera (1 M pixel, Basler A102f). The microscope was adjusted in such a way as to give a spatial resolution of 8 μm per pixel.

The distances between the center of the bubble and the free surface (s_{FS}) and rigid boundary (s_{RB}) are shown schematically in Fig. 2. The rigid boundary was moved using a separated positioning system, while the distance between the free surface and the center of the bubble was varied by changing the focus position of the breakdown laser. The distances between center of the bubble and the boundaries were measured optodynamically using the BDP method, i.e., from the times of flight of the shock-wave reflections.

A. BDP MEASUREMENT AND A COMPARISON WITH SHADOW PHOTOGRAPHY

BDP scanning is based on measurements of the probe-beam deflections at different positions relative to the breakdown region, representing the origin of the cavitation bubble. The deflections are detected with a photodetector providing the BDP signal. From such a signal the time of flight, i.e., the time that it takes for the shock wave or cavitation bubble to reach the probe beam at a particular position, can be obtained. Figure 3 shows some typical BDP signals corresponding to the probe beam being positioned at three different distances relative to the breakdown region [Fig. 3(c)], some results from the BDP scanning [Fig. 3(b)], as well as some typical photos made using shadow photography during the first bubble oscillation [Fig. 3(a)]. The distance between the

Downloaded 08 Nov 2007 to 193.2.7.100. Redistribution subject to AIP license or copyright, see http://jap.aip.org/jap/copyright.jsp

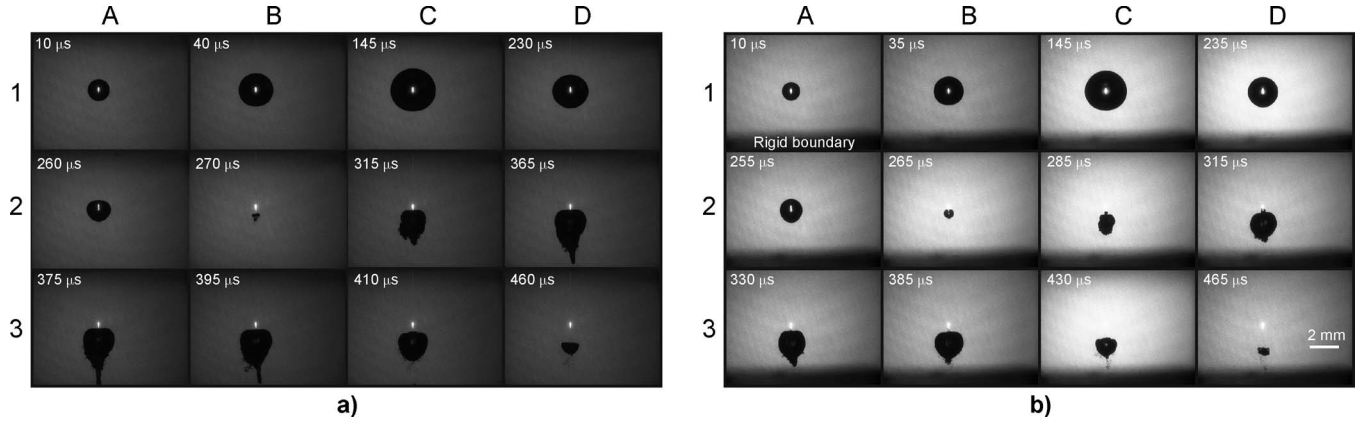

FIG. 4. (a) Images of an oscillating bubble near a free surface ($s_{FS}=4$ mm, $\gamma_{FS}\sim 2.6$). The surface was above the bubble. The bright spot in the center of each frame is plasma, while the black area on the brighter background is a cavitation bubble. (b) Images of an oscillating bubble near a free surface ($s_{FS}=16$ mm, $\gamma_{FS}\sim 10.4$) and a rigid boundary ($s_{RB}=3.3$ mm, $\gamma_{RB}\sim 2.2$). The free surface was above the bubble, while the rigid boundary was below the bubble. The breakdown laser pulse enters from the top of each frame. The scale is shown in frame *D*3.

free surface and the breakdown region was $s_{FS}=8$ mm, while the distance between the rigid boundary and the center of the bubble was $s_{RB}=3.45$ mm.

Figures 3(a) and 3(b) provide a comparison of the shadow photography and the BDP scanning. During BDP scanning the probe-beam position is changed relative to the breakdown center. On the other hand, shadow photography is based on delaying the exposure time relative to the occurrence of the breakdown. Figure 3(a) shows some typical images taken using shadow photography during the first bubble oscillation. Time is represented on the horizontal axis and the dashed lines show the probe beam at some typical positions (vertical axis) during the BDP scanning. It is clear that the top of the expanding bubble crossed the probe beam, positioned 1.06 mm above the center (position 2), 28 μs after the breakdown. At the same time the bottom of the bubble reached position 3 (0.87 mm below the center). Furthermore, the bubble reached its final radius $\sim$140 μs after the breakdown and at the same time it touched the probe positioned 1.55 mm above the center (position 1). When the final radius was achieved the bubble started collapsing in an asymmetrical way. This asymmetry was a consequence of the rigid boundary positioned 3.45 mm below the center of the bubble. Therefore, the probe at position 2 was again reached by the top of the bubble 238 μs after the breakdown. On the other hand, the bottom of the bubble crossed position 3 after an additional 27 μs, i.e., at $t=265$ μs.

Figure 3(b) shows the results obtained with the BDP scanning. The time for each particular probe-beam position was obtained from the beam-deflection signal, with each point being an average of three measurements. The asymmetrical collapse is clearly visible. Typical BDP positions, presented in Fig. 3(a) and described earlier, are also denoted on this graph by the horizontal dashed line and vertical dash-dotted line. A comparison between the shadow photography [Fig. 3(a)] and the BDP measurements [Fig. 3(b)] demonstrates the good agreement between both methods. A more detailed comparison of shadow photography and BDP scanning was made by Petkovsek *et al.*[22]

Figure 3(c) shows typical BDP signals at particular positions. The peak appearing shortly after the breakdown represents the first shock wave, caused by the plasma expansion. This peak is followed by some smaller peaks (the signals that appear between $\sim$0 and $\sim$30 μs) corresponding to the shock-wave reflections from the rigid boundary and the free surface. Subsequent peaks were caused by the cavitation bubble during its expansion (e.g., see positions 2 and 3 at $t=28$ μs) and collapse (e.g., see the peaks at $t=238$ μs—position 2 and at $t=265$ μs—position 3). When the distance between the probe beam and the center of the bubble corresponds to the maximum radius of the cavitation bubble the peaks from the bubble expansion and bubble collapse merge into one (e.g., see the signal from position 1). The signal changes polarity when the probe beam crosses the breakdown region, which is clear from a comparison of the signals from positions 2 and 3. After the collapse the bubble rebounds and a new shock wave (e.g., see the fourth main peak at position 3) is emitted due to the second bubble expansion (e.g., see the fifth main peak at position 3). The oscillations repeat themselves until enough energy is lost due to the emission of a shock wave after every collapse, the viscosity, and the conduction of heat. A detailed description of the BDP signals from the first three bubble oscillations can be found elsewhere.[22]

IV. RESULTS AND DISCUSSION

The presence of a boundary near an oscillating bubble results in an asymmetrical collapse. In addition, a liquid jet that penetrates through the collapsing bubble is formed. In the case of the rigid boundary this jet is directed toward the boundary. On the other hand, if the boundary is a free surface, the jet is directed away from that surface. Figure 4(a) shows some images of an oscillating bubble near a free surface. The surface is located at the top of each frame (see also Fig. 2). The distance between the center of the bubble and the surface was $s_{FS}=4$ mm, corresponding to $\gamma_{FS}\sim 2.6$. In all the frames in Fig. 4 the plasma—visible as a bright spot—roughly denotes the position of the breakdown and can be used to estimate the point of the bubble's origin. The bubble is visible as a dark area on a brighter background. At the maximum radius after the first expansion (frame *C*1) the

Downloaded 08 Nov 2007 to 193.2.7.100. Redistribution subject to AIP license or copyright, see http://jap.aip.org/jap/copyright.jsp

bubble is almost spherical. During the subsequent collapse this symmetry is lost and the top of the bubble is flattened (frame *A*2). In the final stage of the collapse a jet is produced, penetrating the bubble in the direction away from the free surface.[29] This liquid jet becomes visible after the first collapse (images *C*2–*B*3). The shape of the bubble during the second oscillation is very similar to the theoretical predictions of Blake *et al.*[43]

Figure 4(b) shows some typical images captured near a rigid boundary. The distance between the rigid boundary and the center of the bubble was s_{RB}=3.3 mm ($\gamma_{RB}\sim$2.2). The rigid boundary was positioned below the bubble, while the free surface was s_{FS}=16 mm ($\gamma_{FS}\sim$10.4) above the center of the bubble (see Fig. 2). When the bubble collapses in the vicinity of the rigid boundary, the boundary hinders the flow of fluid toward the bubble. As a result a low-pressure region develops between the bubble and the boundary,[24] and this leads to a difference in the pressure between the liquid below and above the bubble, causing a strong acceleration of the bubble's upper wall. The result of this is that a liquid jet is formed and directed toward the rigid boundary. The jet hits the bubble's opposite wall in the final stage of the collapse and penetrates the bubble during the collapse and rebound.[4] From frames *D*2–*C*3 in Fig. 4(b) we can see that it becomes visible during the second oscillation.

Figure 5 shows the movement of the top (squares) and the bottom (circles) of the bubble near the boundaries, as measured with the BDP method. The time for each particular position of the bubble's top/bottom was obtained from the beam-deflection signal corresponding to the current position of the probe beam. Each point is the average of three measurements. The top and the bottom were distinguished in the BDP signals from the polarization of the peaks. As explained in Sec. III A, the polarization reverses when the probe crosses the center of the bubble. The vertical axis in both figures shows the distance relative to the breakdown region. Here, positive signs denote distances above the initial position of the bubble (i.e., breakdown region), while negative signs denote distances under the breakdown region (see also Fig. 2). Figure 5(a) shows the first two oscillations of the cavitation bubble in the vicinity of the free surface. The surface was placed s_{FS}=4 mm ($\gamma_{FS}\sim$2.6) above the center of the bubble. The slope of the graph shows the velocities of the top and bottom of the bubble. Frame *C*2 in Fig. 4(b) shows that the jet is formed on the bottom of the bubble after the rebound. In Fig. 5(a) a liquid jet is visible as an increase in the velocity of the bottom of the bubble (between ~270 and ~290 μs). Its average velocity in the first 5 μs after the rebound was ~170 m/s. The flattening of the top of the bubble is also clearly visible during the second oscillation. The average velocity of the top of the bubble in the first 5 μs after the rebound was ~10 m/s.

Figure 5(b) shows the bubble oscillating between the free surface and the rigid boundary. The free surface was s_{FS}=4 mm ($\gamma_{FS}\sim$2.6) above the breakdown region, while the rigid boundary was s_{RB}=3.5 mm ($\gamma_{RB}\sim$2.3) below the center of the cavitation bubble. Similar effects as in Fig. 5(a) are visible here. The main difference is that the oscillating times are prolonged due to the presence of the rigid boundary. The results from Fig. 5(a) are also shown as black dots for a better comparison. The average velocity of the liquid jet in the first 5 μs after the rebound was ~110 m/s. The top of the bubble is flattened again, since γ_{RB} is larger than 2 and therefore a counterjet cannot be formed.[4]

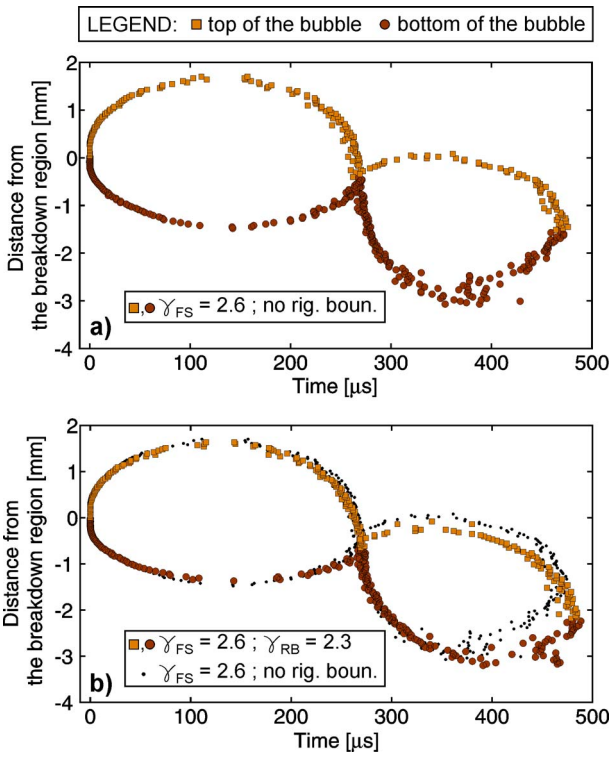

FIG. 5. (Color online) The movement of the top (squares) and the bottom (circles) of the bubble near the boundaries, measured using the BDP method. Each point is the average of three measurements. (a) First two oscillations of a bubble near a free surface (s_{FS}=4 mm, $\gamma_{FS}\sim$2.6). The free surface was placed above the top of the bubble. (b) The first two oscillations of a bubble near a free surface (s_{FS}=4 mm, $\gamma_{FS}\sim$2.6) and a rigid boundary (s_{RB}=3.3 mm, $\gamma_{RB}\sim$2.2). The rigid boundary was placed below the bottom of the bubble. For a better comparison the black dots show the results for a bubble oscillating only near a free surface.

BDP measurements near a rigid boundary were also pre-

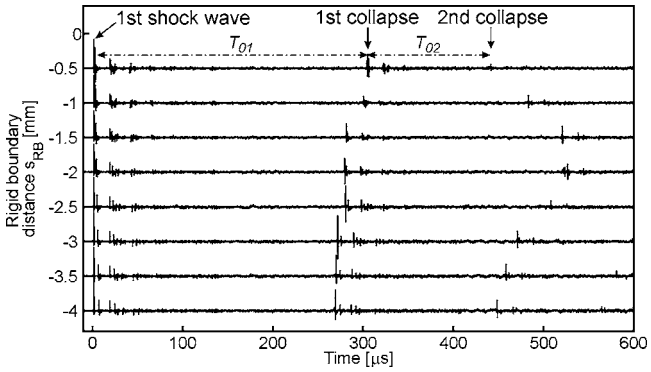

FIG. 6. Typical BDP signals for different distances between the rigid boundary and the center of the bubble. The probe beam was placed 2.7 mm above the center of the bubble. Therefore, only shock-wave signals were visible, since the maximum bubble radius was less than 1.6 mm. Three main peaks on each signal represent the first, second, and third shock waves. The other peaks are shock-wave reflections from the boundaries. The oscillation times T_{01} and T_{02} can be obtained from the difference in the times of flight for the second and first shock waves and from the difference in the times of flight for the third and second shock waves, respectively.

Downloaded 08 Nov 2007 to 193.2.7.100. Redistribution subject to AIP license or copyright, see http://jap.aip.org/jap/copyright.jsp

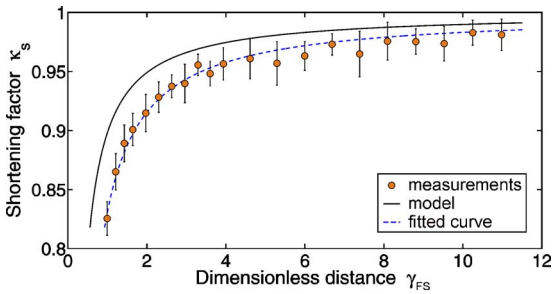

FIG. 7. (Color online) Measurements of the shortening factor κ_s near a free surface. Each point is an average of 40 measurements. The solid line represents the prolongation factor derived from the modified Rayleigh model [Eq. (10)], while the broken curve represents a curve fitted to the experimental results.

formed by Zhao *et al.*,[21] however, their results did not include the bottom of the bubble. Additionally, none of the effects that we observed near a boundary, i.e., the liquid jet or the flattening of the top of the bubble, were reported. On the other hand, our results are similar to measurements of the movement of the top and bottom of the bubble obtained by Vogel *et al.*,[4] who used high-speed photography in their investigations.

Typical BDP signals for different distances between the rigid boundary and the bubble's center are presented in Fig. 6. The probe beam was placed 2.7 mm above the center. For this reason only shock-wave signals were visible, since the maximum bubble radius was less than 1.6 mm. Three main peaks on each signal are as follows: the first shock wave, emitted shortly after the breakdown; the second shock wave, emitted after the first bubble collapse; and the third shock wave, emitted after the second bubble collapse. The other peaks are reflections from the boundaries. Since each signal includes information on all the shock waves emitted from a single bubble, the oscillation times T_{01} and T_{02} can be calculated as the difference in the times of flight for the second and first shock waves and as a difference between the times of flight for the third and second shock waves, respectively. In this way we can measure the shortening and prolongation factors.

The measurements of the shortening factor κ_s near a free surface are presented in Fig. 7. The horizontal axis is used for the dimensionless distance γ_{FS}. Each point is the average of 40 measurements. The bubble's radius in an infinite liquid was $\sim$1.55 mm, which corresponds to a Rayleigh's collapse time $T_C \sim 142$ μs. The solid line represents the prolongation factor derived from the modified Rayleigh model [Eq. (11)], while the broken curve represents the curve fitted to the experimental data. The second term in Eq. (6) shows that the oscillation times are shortened due to the change in the kinetic energy associated with the volume outside the liquid with the oscillating bubble.

The prolongation factors κ_p of a bubble oscillating between a rigid boundary and a free surface were also measured. The results for the oscillation of the first and second bubble are presented in Figs. 8(a) and 8(b), respectively. Two sets of measurements with a fixed distance between the center of the bubble and the free surface were made: the first set (circles) 4 mm ($\gamma_{FS} \sim 2.6$) and the second set (squares) 16 mm ($\gamma_{FS} \sim 10.4$) below the free surface. On the other hand, the distance between the center of the bubble and the rigid boundary was changed and this is represented as a dimensionless distance γ_{RB} on the x axes of both figures. A comparison of the results for both sets of measurements indicates that two effects appeared: the shortening of the oscillation time due to the free surface and the prolongation of the oscillation time due to the rigid boundary. Therefore, in the case of $\gamma_{FS} \sim 2.6$ (circles), the maximum prolongation factors were 1.08 for the first oscillation and 1.32 for the second oscillation. On the other hand, for a larger distance between the free surface and the center of the bubble ($\gamma_{FS} \sim 10.4$) the maximum prolongation factors were 1.14 for the first and 2.63 for the second oscillation, respectively. Similar results were obtained by Brujan *et al.*[13] After that the maximum value of the prolongation factor starts to decrease. We believe that the main reason for the decrease of the oscillation time is the fact that in the limit $\gamma_{RB} \to 0$ the bubble could not exist. On the other hand, for the limit $\gamma_{RB} \to \infty$ the prolongation factor dropped below 1. This effect occurs due to the presence of a free surface. If there was no free surface the oscillation times at that limit should go against the Rayleigh collapse time, i.e., $\kappa_p = 1$.

The solid curve in Fig. 8(a) represents a theoretical curve derived by Rattray[39] [see Eq. (2)]. The broken curves represent the function

$$\kappa = 1 + a/\gamma_{RB} - b; \quad (a,b > 0), \tag{12}$$

fitted to experimental data. The second term in Eq. (12) corresponds to the prolongation of the oscillation time due to the rigid boundary, while the third term corresponds to the shortening of the oscillation time due to the free surface. The last term does not depend on γ_{FS} since the distance between the center of the bubble and the free surface was fixed for each set of measurements.

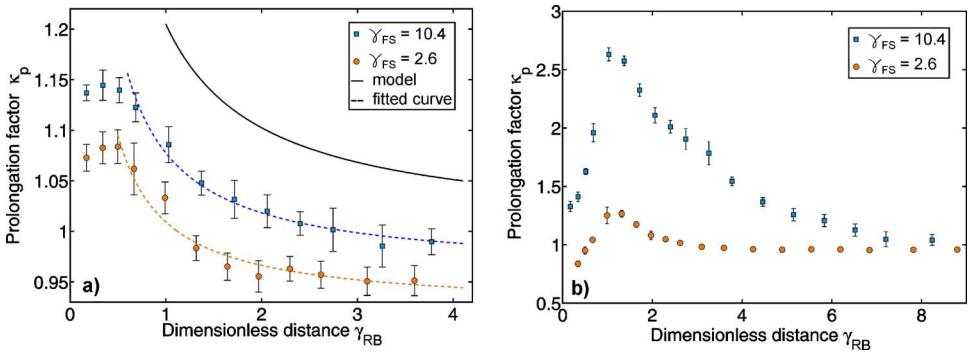

FIG. 8. (Color online) Prolongation factor κ_p near a rigid boundary and a free surface. Two sets of measurements with a fixed distance between the center of the bubble and the free surface were performed: $\gamma_{FS} \sim 2.6$ (circles) and $\gamma_{FS} \sim 10.4$ (squares). (a) Prolongation factor for the first bubble oscillation. The solid line represents Rattray's model [Eq. (2)], and the broken curves show curves [Eq. (12)] fitted to experimental data. (b) Prolongation factor for the second bubble oscillation.

Downloaded 08 Nov 2007 to 193.2.7.100. Redistribution subject to AIP license or copyright, see http://jap.aip.org/jap/copyright.jsp

V. CONCLUSION

We performed BDP measurements on a bubble oscillating between a rigid boundary and a free surface. The results relating to the dynamics of the bottom of the bubble indicated the presence of a liquid jet. The jet was directed away from the boundary in the case of a free surface and toward the boundary when the bubble was oscillating near a rigid boundary. The flatness of the bubble's top was also clear from the BDP measurements.

Using the BDP method we also measured the shortening factor due to the free surface, as well as the prolongation factor due to the rigid boundary. Rayleigh's model was extended and compared to our experimental results in order to explain the shortening of the oscillation times for the bubble oscillating near a free surface. We showed that the oscillation times are reduced due to the change in the kinetic energy associated with the volume outside the liquid with an oscillating bubble. On the other hand, measurements of the prolongation factor showed that two effects appeared when the bubble oscillates between a rigid boundary and a free surface: the shortening of the oscillation time due to the free surface and the prolongation of the oscillation time due to the rigid boundary.

[1]W. Lauterborn, Appl. Phys. Lett. **21**, 27 (1972).
[2]W. Lauterborn and H. Bolle, J. Fluid Mech. **72**, 391 (1975).
[3]A. Vogel and W. Lauterborn, J. Acoust. Soc. Am. **84**, 719 (1988).
[4]A. Vogel, W. Lauterborn, and R. Timm, J. Fluid Mech. **206**, 299 (1989).
[5]A. Vogel, P. Schweiger, A. Frieser, M. N. Asiyo, and R. Bringruber, IEEE J. Quantum Electron. **26**, 2240 (1990).
[6]A. Vogel, S. Busch, and U. Parlitz, J. Acoust. Soc. Am. **100**, 148 (1996).
[7]J. Noack, D. X. Hammer, G. D. Noojin, B. A. Rockwell, and A. Vogel, J. Appl. Phys. **83**, 7488 (1998).
[8]J. Noack and A. Vogel, Appl. Opt. **37**, 4092 (1998).
[9]A. Philipp and W. Lauterborn, J. Fluid Mech. **361**, 75 (1998).
[10]J. C. Isselin, A. P. Alloncle, and M. Autric, J. Appl. Phys. **84**, 5766 (1998).
[11]P. B. Robinson, J. R. Blake, T. Kodama, A. Shima, and Y. Tomita, J. Appl. Phys. **89**, 8225 (2001).
[12]E. A. Brujan, K. Nahen, P. Schmidt, and A. Vogel, J. Fluid Mech. **433**, 251 (2001).
[13]E. A. Brujan, K. Nahen, P. Schmidt, and A. Vogel, J. Fluid Mech. **433**, 283 (2001).
[14]E. A. Brujan, G. S. Keen, A. Vogel, and J. R. Blake, Phys. Fluids **14**, 85 (2002).
[15]S. V. Egerev, Acoust. Phys. **49**, 59 (2003).
[16]Y. Tomita and T. Kodama, J. Appl. Phys. **94**, 2809 (2003).
[17]X. Chen, R. Q. Xu, Z. H. Shen, J. Lu, and X. W. Ni, Opt. Laser Technol. **36**, 197 (2004).
[18]R. Petkovšek, J. Možina, and G. Močnik, Opt. Express **13**, 4107 (2005).
[19]E. A. Brujan and A. Vogel, J. Fluid Mech. **558**, 281 (2006).
[20]T. Kurz, D. Kröninger, R. Geisler, and W. Lauterborn, Phys. Rev. E **74**, 066307 (2006).
[21]R. Zhao, R. Q. Xu, Z. H. Shen, J. Lu, and X. W. Ni, Opt. Laser Technol. **39**, 968 (2007).
[22]R. Petkovšek and P. Gregorčič, J. Appl. Phys. **102**, 044909 (2007).
[23]R. Petkovšek, P. Gregorčič, and J. Možina, Meas. Sci. Technol. **18**, 2972 (2007).
[24]A. Vogel, *Optical Breakdown in Water and Ocular Media, and Its Use for Intraocular Photodisruption* (Shaker Verlag, Aachen, 2001).
[25]L. Rayleigh, Philos. Mag. **34**, 94 (1917).
[26]M. S. Plesset, J. Appl. Mech. **16**, 277 (1949).
[27]T. B. Benjamin and A. T. Ellis, Philos. Trans. R. Soc. London, Ser. A **260**, 221 (1966).
[28]Y. Tomita and A. Shima, J. Fluid Mech. **169**, 535 (1986).
[29]J. R. Blake and D. C. Gibson, J. Fluid Mech. **111**, 123 (1981).
[30]J. R. Krieger and G. L. Chahine, J. Acoust. Soc. Am. **118**, 2961 (2005).
[31]D. Krefting, R. Mettin, and W. Lauterborn, Ultrason. Sonochem. **11**, 119 (2004).
[32]A. Vogel, Phys. Med. Biol. **42**, 895 (1997).
[33]V. Venugopalan, A. Guerra, K. Nahen, and A. Vogel, Phys. Rev. Lett. **88**, 078103 (2002).
[34]K. R. Rau, P. A. Quinto-Su, A. N. Hellman, and V. Venugopalan, Biophys. J. **91**, 317 (2006).
[35]P. Marmottant and S. Hilgenfeldt, Nature (London) **423**, 153 (2003).
[36]P. Prentice, A. Cuschieri, K. Dholakia, M. Prausnitz, and P. Campbell, Nat. Phys. **1**, 107 (2005).
[37]A. Vogel, I. Apitz, S. Freidank, and R. Dijkink, Opt. Lett. **31**, 1812 (2006).
[38]D. Obreschkow, P. Kobel, N. Dorsaz, A. de Bosset, C. Nicollier, and M. Farhat, Phys. Rev. Lett. **97**, 094502 (2006).
[39]M. S. Plesset and R. B. Chapman, J. Fluid Mech. **47**, 283 (1971).
[40]F. Docchio, P. Regondi, M. R. C. Capon, and J. Mellerio, Appl. Opt. **27**, 3669 (1988).
[41]G. P. Davidson and D. C. Emmony, J. Phys E: J. Sci. Instrum. **13**, 92 (1980).
[42]J. Diaci, Rev. Sci. Instrum. **63**, 5306 (1992).
[43]J. R. Blake, A. Pearson, and S. R. Otto, Fourth International Symposium on Cavitation, 2001, pp. 1–8; http://cav2001.library.caltech.edu/.

Downloaded 08 Nov 2007 to 193.2.7.100. Redistribution subject to AIP license or copyright, see http://jap.aip.org/jap/copyright.jsp